applied sciences

MDPI

Article

Influence of Different Carbon Content on Reduction of Zinc Oxide via Metal Bath

Michael Auer *, Christoph Wölfler and Jürgen Antrekowitsch

Nonferrous Metallurgy, Montanuniversität Leoben, 8700 Leoben, Austria; christoph.woelfler@unileoben.ac.at (C.W.); juergen.antrekowitsch@unileoben.ac.at (J.A.)
* Correspondence: michael.auer@unileoben.ac.at

Abstract: Electric arc furnace dust (EAFD) is an important secondary resource for the zinc industry. The most common process for its recycling is the pyro-metallurgical treatment in the Waelz process. However, this process focuses on the recycling of the zinc, whereas the recovery of other metals from the EAFD—such as iron and other alloying elements—is neglected. An up-to-date version of reprocessing can involve multi-metal recycling by means of a metal bath containing carbon. The use of a liquid iron alloy requires a higher processing temperature, which enables the reduction and melting of iron oxides as well as other compounds occurring in the dust. Furthermore, the Zn yield is higher and the reduction kinetics are faster than in the Waelz process. This paper is only focused on the zinc reduction in such a metal bath. In order to determine the influence of the carbon content in the molten metal on the reduction rate, experiments were carried out on the reduction behavior of zinc oxide using a synthetic slag. This slag, with a basicity $B_2 = 1$, was applied to an iron bath with varying carbon contents. (0.85%, 2.16%, 2.89%, and 4.15%) The decrease in the zinc oxide concentration was monitored, along with the reaction rates calculated from these data. It was found that the reaction rate increases with rising carbon content in the melt.

Keywords: electric arc furnace dust; zinc oxide reduction; metal bath

check for updates

Citation: Auer, M.; Wölfler, C.; Antrekowitsch, J. Influence of Different Carbon Content on Reduction of Zinc Oxide via Metal Bath. *Appl. Sci.* **2022**, *12*, 664. https://doi.org/10.3390/app12020664

Academic Editor: Ioanna Vasiliadou

Received: 30 November 2021
Accepted: 4 January 2022
Published: 11 January 2022
Corrected: 21 April 2022

Publisher's Note: MDPI stays neutral with regard to jurisdictional claims in published maps and institutional affiliations.

Copyright: © 2022 by the authors. Licensee MDPI, Basel, Switzerland. This article is an open access article distributed under the terms and conditions of the Creative Commons Attribution (CC BY) license (https://creativecommons.org/licenses/by/4.0/).

1. Introduction

Steel mill dusts with high zinc content, occurring during the production of carbon steel, are a well-known secondary resource for the zinc industry. Because of the heavy metal content in the dust (Pb, Cr, Cd, etc.), the EAFD is categorized as a hazardous waste and, therefore, creates a major issue for the steel producer. Due to environmental concerns, it is important to recycle the dust in a proper way. Despite considerable disadvantages, such as low product quality and high amounts of residual waste, the Waelz process has dominated the recycling of these dusts for several decades. Throughout Europe, more than 90% of the EAFDs are treated in Waelz kilns. Decreasing landfill capacities and increasing disposal costs, along with global rethinking towards a circular economy, have led to significant interest in establishing a new, innovative process concept. The desire for a zero-waste approach and high product quality provides strong motivation for a new recycling route. Therefore, research is focused on multi-metal recovery and a possible application of the final slag in the building industry. A suitable concept could be the recycling of the EAFD via an iron bath containing dissolved carbon. Process developments such as the PIZO, ESRF, and 2sDR processes make use of this technology [1–5].

In characterization studies of electric arc furnace dusts, it should be noted that a large part of the compounds occurring are iron oxide (Fe_2O_3), zinc oxide (ZnO), and zinc ferrite ($ZnO*Fe_2O_3$). Depending on the concentration of the individual elements or the influence of temperature, the ratios between these three species can change, even though the total mass of all compounds remains almost unchanged. It can also be considered that in a neutral atmosphere zinc ferrite decomposes to ZnO and Fe_2O_3 at ~1200 °C, as shown in (1).

Therefore, ZnO*Fe_2O_3 can be neglected at the trial process temperature described in this paper (1400 °C) [1,2,6–16].

$$ZnO \times Fe_2O_{3(s)} = ZnO_{(s)} + Fe_2O_{3(s)} \quad (1)$$

Furthermore, the following experiments focus on the reduction behavior of ZnO, while iron is only considered as an additional reducing agent. For this reason, the reduction reactions of zinc oxide with carbon (C) dissolved in the iron melt, as well as the interactions with iron oxide and metallic iron, are described below. The system can be divided into three areas:

- The metal bath containing the dissolved reducing agent (carbon);
- The slag, including the zinc and iron oxide compounds;
- The gaseous phase above the slag.

At the metal–slag interface, direct reduction occurs with the dissolved carbon in the iron bath as well as with metallic iron. ZnO reacts with Fe from the melt and forms FeO as shown in (2). A similar behavior can be observed in the reaction with dissolved carbon listed in (3). A high C content in the iron bath increases the carbon activity and, therefore, the driving force for the reduction of ZnO [6,7,9,10,17–20].

$$(ZnO) + Fe_{(l)} = Zn_{(g)} + (FeO) \quad (2)$$

$$(ZnO) + [C] = Zn_{(g)} + CO_{(g)} \quad (3)$$

The reduction of zinc oxide by iron is confirmed by the Richardson–Ellingham diagram (RED), which is limited to standard conditions (1 mol of oxygen, ambient pressure of 1 atm, and an activity of 1 for solid and liquid substances). Nevertheless, the RED gives a good overview of the stability of the individual metal oxides, plotting their Gibbs free energy over temperature. Low reaction enthalpies indicate a higher stability of the oxides. Metals that form stable oxides have the characteristics of reducing less stable oxide compounds. In terms of ZnO, the stability is lower than that of FeO at temperatures over 1200 °C. Above this temperature, the reduction of ZnO by iron is thermodynamically possible. In case of carbon, a reduction of zinc oxide can already be carried out at temperatures of at least 1150 °C. Since the selected process temperature is 1400 °C, theoretically the overall reduction rate can be increased, as both reactions occur side by side [21].

The conditions at the slag–gas interface provide the requirements for another reduction with an iron compound, as shown in (4). The low partial pressure of zinc at the boundary layer between the slag and the gas phase favors the reduction of ZnO with FeO [6,19].

$$(ZnO) + 2(FeO) = (Fe_2O_3) + Zn_{(g)} \quad (4)$$

The gaseous components rise through the slag layer, and can react with other compounds in the slag. In addition to Zn, which passes almost unhindered through the slag layer and passes into the gaseous phase, the CO serves as an accelerator for the reduction reactions in the process. The rising CO bubbles increase the reaction area in the system as they react with ZnO, as shown in (5). In addition, the CO bubbles cause a stirring effect that entrains iron particles into the slag, and further increase the reaction surface via an additional reduction path [6,8,10,17,18,22].

$$(ZnO) + CO_{(g)} = Zn_{(g)} + CO_{2\ (g)} \quad (5)$$

In case of reduction reactions with carbon, the Boudouard reaction, as shown in (6), can be added. At the process temperature of 1400 °C, the equilibrium of the Boudouard reaction is predominantly on the product side and, therefore, favors the production of CO. The crucial point is that the thermodynamically preferential reduction reaction of ZnO with the dissolved carbon in the melt (3) can be described as the sum reaction of (5) and (6).

Consequently, the reaction progress and the reduction rate are also related to a fast and efficient expiration of the Boudouard reaction [22–24].

$$C + CO_{2\,(g)} = 2CO_{(g)} \quad (6)$$

To achieve the maximum reduction rate of the Boudourd reaction, the pressure dependence of this reduction and thus of the entire described reduction system plays a desisive role. According to the principle of Le Chatelier, the equilibrium of a reaction tends to shift to reduce changes in reaction parameters. In the case of an increase in pressure, the equilibrium prefers the side of lower molar volume, equivalent to the side of less moles of gas. An increased pressure leads to an equilibrium that tends towards the reactants (CO_2 and C). Therefore, at high pressure, higher temperatures are required for the same amount of CO. The lower number of CO bubbles in the system reduces the reaction area in the slag and limits the mixing between slag and melt. Conversely, a decreased pressure favors the production of CO at lower temperatures and, therefore, leads to a system with a higher reduction potential, meaning the Boudouard reaction is the limiting step for the reduction of zinc oxide [7,17,18].

To sum up the reduction behavior of ZnO on a carbon-containing iron bath, Figure 1 compares the thermodynamic calculations of zinc oxide interacting with carbon and iron. For this purpose, the Gibbs energies are plotted as a function of temperature. The direct reduction with C shows the lowest reaction enthalpy and, therefore, the greatest driving force for the reduction of ZnO, followed by the reductions with Fe, CO, and FeO. With increasing temperature, all reactions show a decrease in delta G, of which the reaction with C again shows the greatest drop. The reaction products Fe_2O_3 and FeO remain in the slag and, in the case of FeO, are available for a further reduction of ZnO at the slag–gas interface. At the slag–melt interface, a reduction of ZnO via liquid iron can occur. The reaction product—gaseous zinc—forms bubbles just as CO does, produced during carbothermic reduction. Carbon monoxide can be oxidized again in the slag, forming CO_2 via the reduction of ZnO. The reaction between FeO and ZnO can only arise in areas with very low Zn partial pressure. The sole interface that meets these requirements is the boundary layer between the atmosphere and the slag. In case of the experiments carried out in this paper, the gaseous Zn is directly re-oxidized above the melt and transferred into the off-gas system. As a result, the reaction equilibrium of all reactions is shifted to the production of $Zn_{(g)}$. The reduction of ZnO by FeO, which shows positive Gibbs energy between 1200 and 1700 °C, can therefore also occur during the experiments shown in this paper. [6,10,20,21,24]

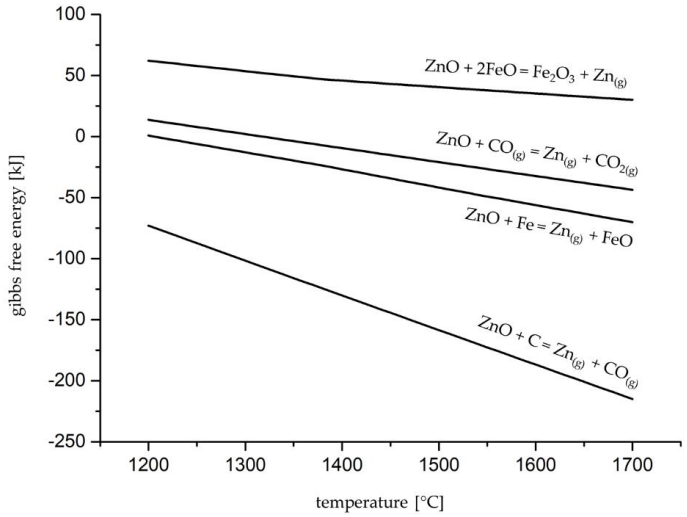

Figure 1. Change in free enthalpy of reaction with increasing temperature for possible zinc oxide reactions.

2. Materials and Methods

Based on the knowledge described above, a series of laboratory-scale trials were executed to investigate the influence of the initial carbon concentration in the metal bath on the reduction kinetics of zinc oxide. For this reason, reduction experiments were performed on iron baths with defined starting concentration of carbon. A synthetic slag with basicity $B_2 = 1$ was used to simulate process conditions as they occur during the recycling of steel mill dust. The separate addition of zinc oxide defined the initial concentration of ZnO in the slag. The resulting slag and iron samples were analyzed by using SEM–EDX and spark spectrometry.

The tests were carried out in the "Indutherm MU700" induction furnace with a maximum power input of 12 kW at the Chair of Nonferrous Metallurgy of the Montanuniversität Leoben. Heating was provided by a graphite crucible with the following dimensions:

- External dimensions (height: 170 mm; diameter: 110 mm);
- Internal dimensions (height: 140 mm; diameter: 56 mm);
- Thermal isolation of the crucible was secured by a ceramic shell of 7 mm.

Since the experiments were investigating the influence of the carbon concentration in the molten iron on zinc oxide reduction, the experimental setup had to be designed to prevent any contact between the metal bath and the graphite crucible. For this reason, a spinel crucible (70% Al_2O_3, 30% MgO; height: 85 mm; external diameter: 56 mm; thickness: 3 mm) was placed within the graphite crucible. This setup provided uniform, indirect heating of the spinel crucible through the graphite, and protected against additional carbon input. The temperature was measured using a thermocouple placed at the bottom of the graphite crucible. The schematic experimental setup is shown in Figure 2.

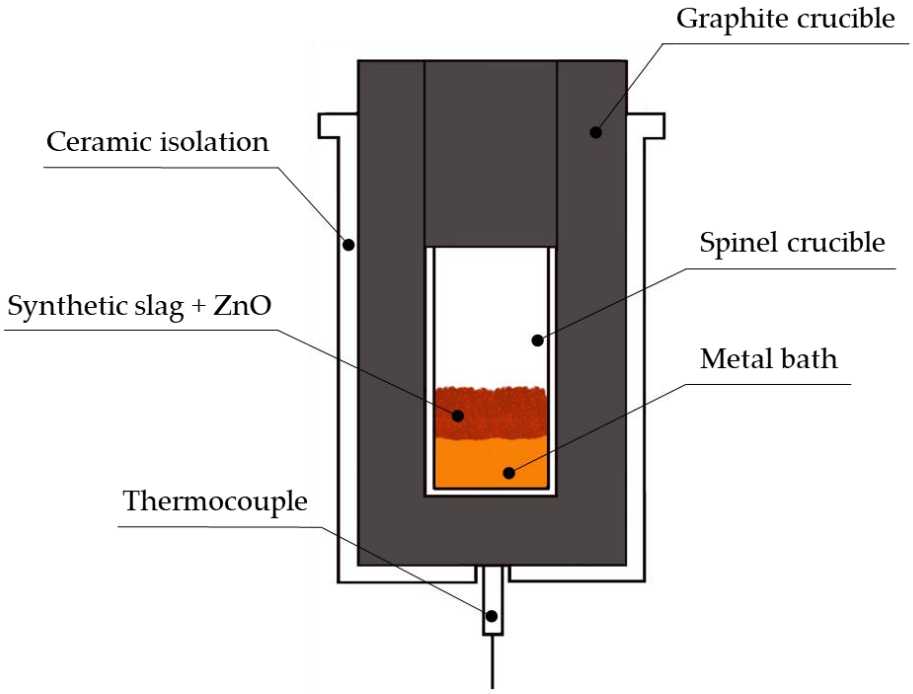

Figure 2. Experimental setup.

The required metal bath was created by melting a pre-produced iron–carbon alloy with a defined C content. After heating the metal bath to 1400 °C, the previously produced synthetic slag was added. The composition of the synthetic slag was based on the slag components occurring in steel mill dusts and thermodynamic calculations ensuring the lowest possible melting point of the slag. After 10 min of temperature homogenization, the zinc oxide was added. The charging of ZnO into the liquid slag was also defined as the starting point of the experiments. The measured temperature at the bottom of the crucible

was set to 1400 °C throughout the entire test period. The compositions of the synthetic slag and zinc oxide are shown in Tables 1 and 2, respectively. Since the crucible was not sealed, the produced gaseous zinc was directly re-oxidized in the furnace atmosphere, and ZnO was transferred into the off-gas system.

Table 1. Chemical composition of the synthetic slag.

Composition of the Synthetic Slag				
Compound	**MgO**	**Al_2O_3**	**SiO_2**	**CaO**
wt-%	0.42	15.57	42.29	41.72

Table 2. Chemical composition of the zinc oxide.

Cofmposition of Zinc Oxide						
Compound	**FeO**	**Al_2O_3**	**SiO_2**	**ZnO**	**PbO**	**CaO**
wt-%	2.17	0.68	0.21	89.16	5.96	1.82

To show the temporal progression of ZnO concentration, the fully reproducible experiments were stopped at defined process times. After completion of the individual trials, the compositions of the slag and the iron–carbon alloy were analyzed. The series of tests included 4 different carbon concentrations in the iron alloy (0.85%. 2.16%, 2.89%, and 4.15%), and the time intervals of the experiments were set to 2, 4, 6, 10. and 15 min. The amounts of the individual components used for the experimental procedures are given in Table 3, and resulted in an initial concentration of ZnO in the slag of 10.55%.

Table 3. Amounts of used input materials.

Input Materials			
Compound	**Iron Alloy**	**Slag**	**Zinc Oxide**
Mass [g]	100	22.35	3

3. Results

The temporal progression of ZnO in the slag, relative to the carbon content in the metal bath, is shown in Figure 3. An increased carbon concentration in the molten iron led to a faster decrease in ZnO in the first six minutes of the test. Additionally, the tests with higher C content in the metal bath showed an earlier formation of a plateau in the trend line. The level of the equilibrium concentration was in a similar range for the experiments with 2.16% C, 2.89% C, and 4.15% C (~2% ZnO). The trial with the lowest carbon concentration in the molten iron showed higher ZnO content after 15 min of process time. Therefore the 15-minute test with a C content of 0.85% could not be used for the analysis of the reaction kinetics, because of unrepresentative conditions during the trial.

Furthermore, the tests with 0.85% carbon have limited significance. Considering the iron–carbon diagram, an iron alloy with 0.85% carbon content is not fully liquid at a temperature of 1400 °C. Although the iron alloy used for the experiment contains some alloying elements, which reduce the melting point (carbon equivalent = 1.15%), it is still present in the 2-phase liquid/solid area. Therefore, the transfer of carbon into the slag is limited. With decreasing carbon content during the reduction of ZnO, the liquidus temperature increases and the proportion of the solid phase rises further. Based on these facts, the test trials using the iron alloy with a carbon content of 0.85% can only be considered in a limited manner.

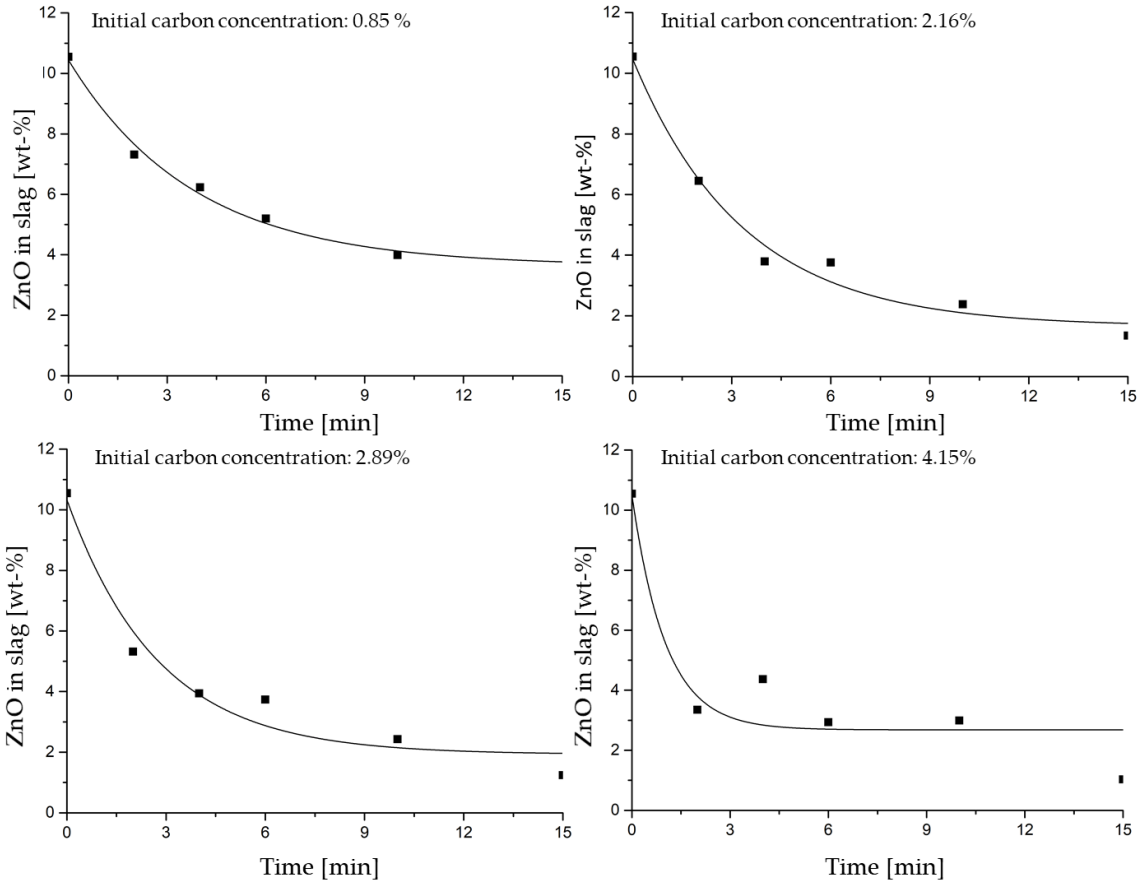

Figure 3. Changes in the zinc oxide content of the slag.

For better illustration of the influence of the carbon concentration in the molten iron on the reaction of ZnO, the reduction rate was calculated from the experimental data. The trend lines correspond to a first-order reaction equation fitting the experimental data. The first-order reaction equation is shown in (7); the derivative, shown in (8), allows the calculation of the reaction rate [24,25].

$$[\mathrm{ZnO}]_{(t)} = [\mathrm{ZnO}]_{(0)} - \mathrm{A} + \mathrm{A} \times \mathrm{e}^{-\mathrm{kt}} \quad (7)$$

$$\mathrm{r}_{(t)} = -\frac{\mathrm{d}[\mathrm{ZnO}]_{(t)}}{\mathrm{dt}} \quad (8)$$

$[\mathrm{ZnO}]_{(t)}$: ZnO content in the slag at time t (%);
$[\mathrm{ZnO}]_{(0)}$: Initial ZnO content in the slag (%);
A: Reaction constant (%);
k: Reaction constant (min^{-1});
t: Time (min);
$\mathrm{r}_{(t)}$: Reaction rate at time t (%/min).

The different concentration trends of ZnO in the slag resulted in various reaction rates, depending on the carbon concentration in the metal bath. The mathematical descriptions of the trend lines and the reaction rates calculated are shown in Table 4.

Table 4. Calculated changes in the concentration of zinc oxide in the slag, and the reaction rates.

C_0 in Metal [%]	ZnO Concentration [%]	Reaction Rate [%/min]
0.85	$[ZnO] = 3.67391 + 6.83081 \times e^{-0.26874 \times t}$	$r = 1.83571 \times e^{-0.26874 \times t}$
2.16	$[ZnO] = 1.66117 + 8.86756 \times e^{-0.30131 \times t}$	$r = 2.67188 \times e^{-0.30131 \times t}$
2.89	$[ZnO] = 1.93761 + 8.45855 \times e^{-0.3673 \times t}$	$r = 3.10683 \times e^{-0.3673 \times t}$
4.15	$[ZnO] = 2.68455 + 7.89179 \times e^{-98.022 \times t}$	$r = 7.73569 \times e^{-98.022 \times t}$

Plotting the reaction rate against the ZnO concentration in the slag results in the curves shown in Figure 4. The different graphs represent the various carbon concentrations in the molten iron. The reaction rates at the beginning of the tests are strongly dependent on the initial concentration of C in the metal bath. At 10% ZnO in the slag, the experiment using the iron bath with 4.15% carbon shows a reaction rate more than four times higher than that with 0.85% carbon. The low reactivity can be justified by the high melting point of an iron alloy with 0.85% carbon. The rate of ZnO reduction is significantly increased at a carbon content of 2.16%, compared to that at 0.85%; however, the difference at 10% ZnO is relatively small, at less than 0.8%/min. The difference between the experiments with C contents of 2.16% and 2.89% is even smaller (0.5%/min), the main reason being their very similar carbon concentrations. As the ZnO concentration in the slag is reduced, the reaction rates of all trials decrease linearly, and converge at lower concentrations of ZnO in the slag. At a residual content of 4% zinc oxide in the slag, the reaction rates of all tests are below 2%/min, and subsequently drop to zero.

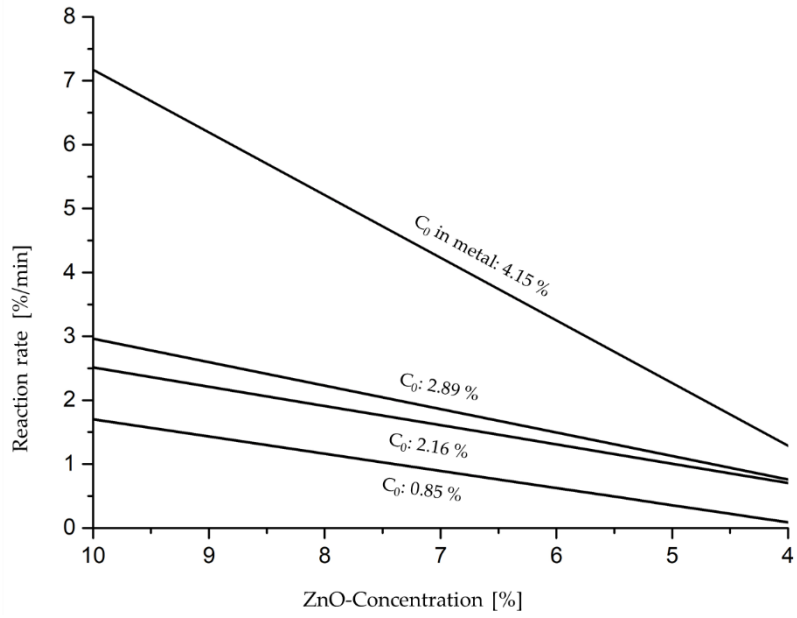

Figure 4. Comparison of reaction rates over the concentration range of 10% to 4%.

The most important aspect of the experiments presented in this paper is that the unwanted carbon input to the melt could be prevented. For this reason, in addition to the analyses of the slag, the C content in the metal bath was also determined after each test. The results and a trend line for each series of trials are shown in Figure 5. Similar to the highest reduction rates of ZnO taking place during the period of 0–6 min, the decrease in carbon concentration in the molten iron is also the greatest during this time. The rest of the process time shows constant C contents, indicating that an undesirable input of carbon to the metal bath could be prevented. The reduction of ZnO, which still occurs between 6 and 15 min, is not evident in the graphs. The large ratio of iron bath to slag means that

the amount of carbon needed for the reduction of the remaining amounts of ZnO causes insignificant changes in the C concentration. The large metal/slag ratio was necessary in order to prevent limitation of the reduction process of ZnO by low amounts of C in the system. The decrease in carbon concentration in all test trials followed a similar temporal progression, and showed no unusual effects in the iron bath.

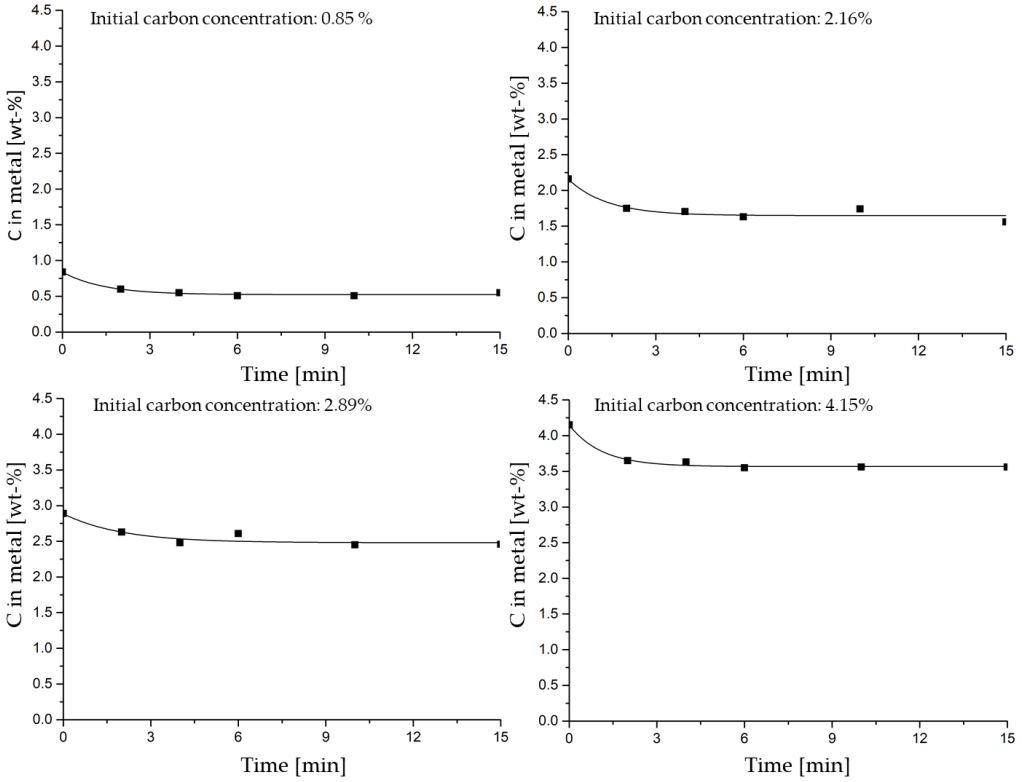

Figure 5. Changes in carbon concentration in the molten iron.

In the tests carried out, the main reduction agent was carbon although, as described previously, zinc oxide can also be reduced by means of iron. This iron-reduced zinc oxide represents only a small proportion of the total mass of reduced zinc.

4. Conclusions

The investigations carried out in this paper confirm that the carbon content in the iron alloy plays a significant role in the reaction process. An effective and fast reduction of a ZnO-containing steel mill dust in a metal bath is ensured by a high carbon concentration in the iron alloy. In the case of an industrial process, two opportunities to secure high C content should be discussed: The first involves using a high ratio of metal to slag in order to achieve the same phenomenon as in the laboratory tests. The changes in the carbon content in the iron alloy, due to the reduction of a certain amount of steel mill dust, differ only slightly from the starting concentration and, therefore, have a negligible influence on the reduction rate. After tapping the slag, the metal bath is carburized by charging a carbon carrier onto the molten metal, and the reduction process can be repeated. The second option would be a permanently installed injection system that provides a continuous supply of carbon to the metal bath. In this case, the C-containing feed material can be provided by an injection lance from above through the slag layer. Furthermore, purging stones installed at the bottom of the furnace and operating with inert gas can increase the movement in the bath, resulting in a higher reaction surface between the melt and the slag, which increases the reduction kinetics to the highest possible value. Using these mechanisms, an economic and ecological process performance with a zinc yield well above 95% is feasible.

At industrial plants, continuous carburization of the melt is preferred, because the melting unit can be kept small and, therefore, the investment costs kept low. Furthermore, the injection device provides an additional stirring effect in the melt, and improves the conditions for an effective and fast reduction of the steel mill dust.

Author Contributions: Conceptualization, M.A. and J.A.; data acquisition, M.A. and C.W.; investigation, M.A. and C.W.; methodology, M.A. and J.A.; project administration, J.A.; supervision, J.A.; writing—original draft preparation, M.A. and C.W.; writing—review and editing, M.A., C.W., and J.A. All authors have read and agreed to the published version of the manuscript.

Funding: COMMBY is an FFG Austria COMET project. We would like to give thanks to the funders Österreichische Forschungsfördergesellschaft (FFG), Steirische Wirtschaftsförderungsgesellschaft 8SFG), Wirtschaft Burgenland GmbH, Land Steiermark, und Land Burgenland.

Institutional Review Board Statement: Not applicable.

Informed Consent Statement: Not applicable.

Data Availability Statement: The data presented in this article are available on request from the corresponding author.

Conflicts of Interest: The authors declare no conflict of interest.

References

1. Antrekowitsch, J.; Rösler, G.; Steinacker, S. State of the Art in Steel Mill Dust Recycling. *Chem. Ing. Tech.* **2015**, *87*, 1498–1503. [CrossRef]
2. Gerald, S.; Jürgen, A.; Christoph, P. Development of a New Recycling Process for High Zinc Containing Steel Mill Dusts including a Detailed Characterization of an Electric Arc Furnace Dust. *BHM Berg-Und Hüttenmännische Mon.* **2012**, *157*, 1–6. [CrossRef]
3. Nyirenda, R.L. The processing of steelmaking flue-dust: A review. *Miner. Eng.* **1991**, *4*, 1003–1025. [CrossRef]
4. Chen, W.-S.; Chou, W.-S.; Tsai, M.-S. Status of EAF Dust Management in Taiwan. *J. Korean Inst. Resour. Recycl.* **2011**, *20*, 3–13. [CrossRef]
5. Advances in waste management. In Proceedings of the 4th WSEAS International Conference on Waste Management, Water Pollution, Air Pollution, Indoor Cli-mate (WWAI '10), Sousse, Tunisia, 3–6 May 2010; Characterication of Steel Mill Electric-Arc Furnace Dust. World Scientific and Engineering Academy and Society, WSEAS Press: Sousse, Tunisia, 2010. ISBN 9789604741908.
6. Pickles, C.A. Reaction of electric arc furnace dust with molten iron containing carbon. *Miner. Processing Extr. Metall.* **2003**, *112*, 81–89. [CrossRef]
7. Bafghi, M.S.; Karimi, M.; Adeli, M. A kinetic study on the carbothermic reduction of zinc oxide from electric arc furnace dust. *Iran. J. Mater. Sci. Eng.* **2013**, *10*, 18–30.
8. Pickles, C.A. Thermodynamic analysis of the selective carbothermic reduction of electric arc furnace dust. *J. Hazard. Mater.* **2008**, *150*, 265–278. [CrossRef] [PubMed]
9. Zhou, Y.; Wu, L.; Wang, J.; Wang, H.; Dong, Y. Separation of ZnO from the Stainless Steelmaking Dust and Graphite Mixture by Microwave Irradiation. *High Temp. Mater. Processes* **2014**, *34*, 177–184. [CrossRef]
10. Pickles, C.A. Thermodynamic Analysis of the Selective Reduction of Electric Arc Furnace Dust By Carbon Monoxide. *High Temp. Mater. Processes* **2007**, *26*, 79–91. [CrossRef]
11. Nakayama, M. New Eaf Dust Treatment Process: ESRF. Available online: http://steelplantech.com/wp-content/uploads/2013/11/201105_EAF_DustTreatment_byNewProcess.pdf (accessed on 4 November 2021).
12. Sofilić, T.; Rastovcan-Mioc, A.; Cerjan-Stefanović, S.; Novosel-Radović, V.; Jenko, M. Characterization of steel mill electric-arc furnace dust. *J. Hazard. Mater.* **2004**, *109*, 59–70. [CrossRef] [PubMed]
13. Dutra, A.; Paiva, P.; Tavares, L.M. Alkaline leaching of zinc from electric arc furnace steel dust. *Miner. Eng.* **2006**, *19*, 478–485. [CrossRef]
14. Steinlechner, S.; Schneeberger, G.; Antrekowitsch, J. Possibilities for the Improvement of Secondary Zinc Oxide Quality. 2011. Available online: https://www.researchgate.net/publication/236006429_Possibilities_for_the_Improvement_of_Secondary_Zinc_Oxide_Quality (accessed on 4 November 2021).
15. Antrekowitsch, J.; Steinlechner, S. The recycling of heavy-metalcontaining wastes: Mass balances and economical estimations. *JOM* **2011**, *63*, 68–72. [CrossRef]
16. Kongoli, F.; Gomez-Marroquin, M.-C.; Contrucci, M.; Lacerda, N.; Cancado, F.V.; de Souza, M.; Valladares, R. (Eds.) Steel Mill Dust—Only a Zinc Resource or a Potential Material for Multi Metal. Recycling? Flogen Star Outreach: Mount Royal, QC, Canada, 2018; ISBN 978-1-987820-82-9.
17. Kim, B.-S.; Yoo, J.-M.; Park, J.-T.; Lee, J.-C. A Kinetic Study of the Carbothermic Reduction of Zinc Oxide with Various Additives. *Mater. Trans.* **2006**, *47*, 2421–2426. [CrossRef]

18. Guger, C.E.; Manning, F.S. Kinetics of zinc oxide reduction with carbon monoxide. *Met. Mater. Trans. B* **1971**, *2*, 3083–3090. [CrossRef]
19. Donald, J.R.; Pickles, C.A. A Kinetic study of the reaction of zinc oxide with iron powder. *Met. Mater. Trans. B* **1996**, *27*, 363–374. [CrossRef]
20. Donald, J.; Pickles, C. Reduction of electric arc furnace dust with solid iron powder. *Can. Metall. Q.* **1996**, *35*, 255–267. [CrossRef]
21. Pawlek, F. *Metallhüttenkunde*; De Gruyter: Berlin, Germany, 1983; ISBN 3-11-007458-3.
22. Chen, H.-K. Kinetic study on the carbothermic reduction of zinc oxide. *Scand J. Metall.* **2001**, *30*, 292–296. [CrossRef]
23. Wu, C.-C.; Chang, F.-C.; Chen, W.-S.; Tsai, M.-S.; Wang, Y.-N. Reduction behavior of zinc ferrite in EAF-dust recycling with CO gas as a reducing agent. *J. Environ. Manag.* **2014**, *143*, 208–213. [CrossRef] [PubMed]
24. Rankin, W.J.; Wright, S. The reduction of zinc from slags by an iron-carbon melt. *Met. Mater. Trans. B* **1990**, *21*, 885–897. [CrossRef]
25. Atkins, P.; de Paula, J. *Physical Chemistry*, 8th ed.; Oxford University Press: Oxford, UK, 2006; ISBN 0-7167-8759-8.